Discrete frictional- and wing-crack based damage model for salt rock

X. Shen & C. Arson

School of Civil and Environmental Engineering, Georgia Institute of Technology, Atlanta, Georgia

J. Ding, F. M. Chester, & J. S. Chester

Center for Tectonophysics, Department of Geology & Geophysics, Texas A&M University, College Station

ABSTRACT: A Discrete Frictional Wing Crack Damage (DFWCD) model is proposed to simulate the initiation and propagation of inter-granular cracks in salt rock undergoing semi-brittle deformation at low mean stress. Damage is defined as the integration of crack densities over the unit sphere. In order to simulate inter-crystalline bonding, a cohesive frictional model is formulated for main cracks. Crack growth is controlled by mode I and mode II fracture mechanics criteria. Salt crystals are rhomboids, so we assume that wing cracks are perpendicular to the main cracks. The tensile normal stress triggers the growth of wing cracks according to a mode I fracture mechanics criterion. The formulated DFWCD model is calibrated against triaxial cyclic loading tests. Our model can predict the microstructure development, the non linear-stress/strain relationship and the stiffness degradation during the cyclic loading.

1 INTRODUCTION

Salt rock is a polycrystalline material made of bonded crystals. Due to its low permeability, low porosity and creep properties, salt rock is usually considered as a favorable material for geological storage, such as CO₂ sequestration and nuclear waste confinement (e.g., Waste Isolation Pilot Plant, WIPP). Under typical geostorage stress conditions, the initiation and propagation of defects leads to a degradation of stiffness and a decrease of strength in the host rock. In this paper, a multi-scale mechanical model is proposed to predict the development of microstructure, stiffness, and deformation under cyclic loading.

Damage Continuum Mechanics provides a theoretical framework to model damage (and the resulting loss of stiffness and strength) in solids (Lemaitre & Desmorat, 2005). The fundamental idea is that crack propagation leads to a loss of potential strain energy. The stress-strain relationship is derived from the postulated expression of a thermodynamic potential, and the evolution of damage is related to phenomenological driving forces, such as tensile strains (Cicekli, et al., 2007; Arson & Gatmiri, 2011). Under the assumption of crack noninteraction, the damage variable is commonly defined as the second-order crack density tensor (Kachanov, 1992; Zhu & Arson, 2015).

In micromechanical models, the macroscopic effective properties are related directly to the evolution of microscopic cracks. The mechanical behavior of the damaged REV is calculated based on the displacement jumps across crack faces (Budiansky and O'Connell, 1976; Kachanov, 1992; 1993). Based on fracture mechanics principles, the initiation, propagation, opening, closure and frictional sliding of micro-cracks in

homogeneous media was studied in Mode I (Krajcinovic et al., 1991), Mode II (Gambarotta & Lagomarsino, 1993) and mixed-Mode with wing crack development (Nemat-Nasser & Obata, 1988, Jin & Arson 2017). Wing cracks are the tensile microcracks that stem from frictional defects in rock (Lehner, 1996).

The stiffness of a polycrystalline material is less than that of a single crystal. Grain-boundary microscopic cracks are thus more likely to initiate and propagate than intra-granular cracks, particularly at low mean stress for a semi-brittle material (Ding et al., 2017). During triaxial tests at low mean stress, the deformation and stiffness reduction of salt rock samples are mostly due to grain rearrangement and damage development along grain contacts (Fig.1). In particular, wing cracks form at the tips of pre-existing defects.

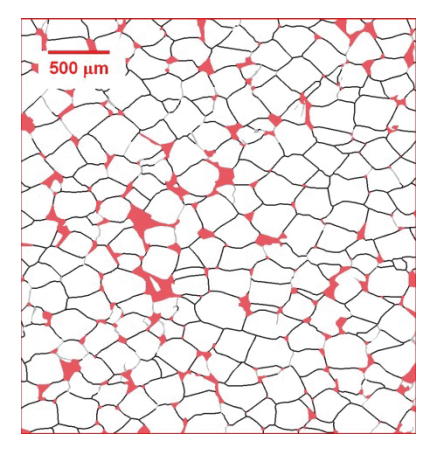


Figure 1. Microstructure map of experimentally-deformed, granular salt rock after 2.3% axial strain. The cracks and voids are shown in gray and red respectively (Ding et al., 2017).

In the following, a Discrete Frictional Wing Crack Damage (DFWCD) model is proposed, based on micromechanics and CDM principles. In

Section 2, we give the expression of the Gibbs free energy, and we provide the relationship between the REV elastic stiffness and the densities of main and wing cracks. In Section 3, damage criteria and flow rules for both main cracks and wing cracks are proposed to predict the growth of micro-cracks. In section 4, the DFWCD model is calibrated against a triaxial cyclic loading test, and the evolution of damage is simulated.

2 GIBBS FREE ENERGY

2.1 Microscopic main cracks modes

We use a dilute scheme, in which the interaction between main cracks is negligible. The total stress in the REV, noted σ , is the average of the stress in the cracks (σ _c) and of the stress in the matrix (σ _m).

$$\sigma = \frac{1}{V_{REV}} \int_{V_{REV}} \left[\sigma_c(x) + \sigma_m(x) \right] dx \tag{1}$$

Under static conditions, the cracks stress σ_c is in self-equilibrium, and the stress of the matrix σ_m is equal to the total stress. The normal stress on the cracks, noted σ_n^m , is thus calculated as:

$$\sigma_n^m = \sigma : (\vec{n}_i \otimes \vec{n}_i) \tag{2}$$

where \vec{n}_i is the normal direction of crack plane *i*. The projection of σ in the tangential direction of the crack planes is:

$$\sigma_i^m = \sigma : \vec{n}_i - (\vec{n}_i \cdot \sigma \cdot \vec{n}_i) \vec{n}_i$$
 (3)

Main cracks are assumed to be embedded in a homogeneous matrix. Based on the normal stress and tangential stress conditions, main cracks can develop in either mode I or mode II, according to 5 possible mechanisms. The corresponding deformation modes are described below.

In mode 1, the normal stress is positive: $\sigma_n^m > 0$; the shear stress σ_t^m is smaller than the cohesion of main cracks c, and σ_t^m has never exceeded c during the past loading history. The main crack can open due to normal displacements, but without shear strain.

In mode 2, $\sigma_n^m < 0$; $\sigma_t^m < c$, and σ_t^m has never exceeded c during the past loading history. The main crack is closed, and shear strain does not occur.

In mode 3, $\sigma_n^m > 0$; $\sigma_t^m > c$, or σ_t^m has exceeded c during the past loading history. Normal and shear displacements can occur at the faces of the main cracks.

In mode 4, $\sigma_n^m < 0$; $\sigma_t^m > c$, or σ_t^m has exceeded c during the past loading history, and at the same time, the sum of σ_t^m and frictional stress $\mu \sigma_n^m$ is positive (in which μ is the frictional

coefficient). The main crack is compressed, and shear strain is observed.

In mode 5, $\sigma_n^m < 0$; $\sigma_t^m > c$, or σ_t^m has exceeded c during the past loading history, but $\sigma_t^m + \mu \sigma_n^m < 0$. The main crack is under compressive stress, and shear strain does not occur. But the cohesion due to inter-crystal bonds is set to zero (i.e., bonds are broken).

Cracks are assumed to be penny-shaped. We define crack families, in which all cracks have the same orientation (i.e. same crack plane normal direction) \vec{n}_i and same radius a_i . The volume fractions of the normal and shear displacement jumps of the main cracks are given as follows (Kachanov et al., 2013):

$$\beta_i^m = \rho_i^m s_o N_i^m \sigma_{ni}^m \tag{4}$$

$$\gamma_i^m = \rho_i^m s_1 T_i^m B_i \sigma_{ni}^m \tag{5}$$

where ρ_i^m is the crack density; s_0 and s_1 are the normal and shear elastic compliances of the crack, respectively; N_i^m is the normal mode coefficient; T_i^m is the tangential mode coefficient; B_i is the frictional mode coefficient. N_i^m , T_i^m , and B_i depend on the deformation mode of the main cracks as explained in Table 1. We have:

$$\rho_i^m = \frac{M_i \left(a_i^m\right)^3}{V_{perv}} \tag{6}$$

where M_i is the number of cracks in family i; V_{REV} is the volume of REV.

$$s_o = \frac{16\left(1 - \nu_o^2\right)}{3E} \tag{7}$$

$$s_1 = \frac{32(1 - v_o^2)}{3(1 - 2v_o)E_c} \tag{8}$$

where v_o is the Poisson ratio; E_o is the Young's modulus (Kachanov 1992).

Table 1. Deformation mode coefficients.

Mode	N_i^m	T_i^m	B_{i}
1	1	0	0
2	0	0	0
3	1	1	1
4	0	1	$1 + \mu \sigma_n^m / \ \sigma_t^m\ $
5	0	1	0

2.2 Evolution of wing cracks

The propagation of wing cracks in solids under compression was studied experimentally (Germanovich et al., 1994), numerically (Scholtès and Donzé, 2012), and theoretically (Dyskin and Salganik, 1987), and tensile wing cracks were assumed to initiate at the tip of sliding cracks. The shear force at the main cracks is thus adopted here

as the driving force for the propagation of wing cracks. As salt crystals are typically rhomboids, we assume that wing cracks are always perpendicular to the main cracks, as shown in Fig.2.

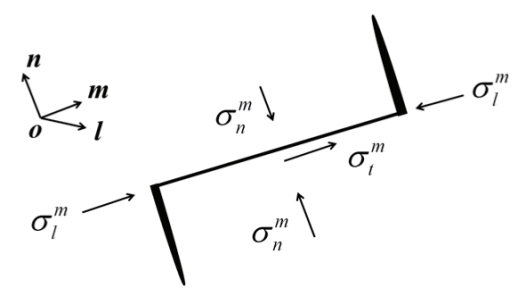


Figure 2. Wing crack propagation model.

The propagation of wing cracks is triggered by a stress in the direction \vec{m} , as shown in Fig.2. This compression direction can be calculated as:

$$\vec{m}_{i} = \frac{\sigma_{ii}^{m}}{\left\|\sigma_{ii}^{m}\right\|} \tag{9}$$

The normal force on a wing crack is sum of the shear force transferred from the main cracks and the projection of force in the direction of \bar{m} from the matrix. With the assumption that the normal stress is uniformly distributed on the wing crack plane, the normal stress of the wing crack is given as:

$$\sigma_{ni}^{w} = \left(\frac{a_{i}^{m}}{a_{i}^{w}}\right)^{2} B_{i} \left\|\sigma_{ii}^{m}\right\| + \sigma_{li}^{m} \tag{10}$$

$$\sigma_{i}^{m} = \vec{m}_{i} \cdot \sigma \cdot \vec{m}_{i} \tag{11}$$

Similarly to Eq.(4) for main cracks, the volume fraction of the normal displacement jumps of a wing crack can be calculated as

$$\beta_i^w = \rho_i^w s_o \sigma_{ni}^w \tag{12}$$

2.3 Expression of the Gibbs free energy

The Helmholtz free energy Ψ_s^* of the REV is the sum of the elastic deformation energy of the matrix and the energy stored in displacement jumps of the main and wing cracks:

$$\Psi_s^* = \frac{1}{2} \varepsilon_o : C_o : \varepsilon_o + \frac{1}{2} \sigma^c : \varepsilon^c$$
 (13)

where ε_0 is the strain of matrix; and ε^c is the strain of cracks. Based on Legendre transformation, the Gibbs free energy can be written as:

$$G^* = \sigma : \varepsilon^E - \Psi_s^* \tag{14}$$

where $\varepsilon^{E} = \varepsilon_{0} + \varepsilon^{c}$ is the elastic strain of REV. The expression of Gibbs energy can be rewritten as:

$$G^* = \frac{1}{2}\sigma : S_o : \sigma + \frac{1}{2}\sigma : \varepsilon_i^m + \sigma : \varepsilon_i^m - \frac{1}{2}\sigma_w^c : \varepsilon_i^w$$
 (15)

$$\varepsilon_i^m = \beta_i^m \vec{n}_i \otimes \vec{n}_i + \frac{1}{2} \left(\gamma_i \otimes \vec{n}_i + \vec{n}_i \otimes \gamma_i \right) \tag{16}$$

$$\varepsilon_i^w = \beta_i^w \vec{m}_i \otimes \vec{m}_i \tag{17}$$

where ε^{m} is the strain of a main crack; ε^{w} is the strain of a wing crack. According to Bazant's discrete integration scheme with 72 elementary directions in the unit sphere (Bazant & Oh 1986), the Gibbs energy integrated with a distribution of cracks orientations can be expressed as:

$$\begin{split} G^* &= \frac{1}{2}\sigma: S_o: \sigma + \frac{1}{2}\sum_{i=1}^{\mathcal{Q}} w_i \{s_o \rho_i^m N_i^m (\vec{n}_i \cdot \sigma \cdot \vec{n}_i) (\vec{n}_i \cdot \sigma \cdot \vec{n}_i) \\ &+ s_1 \rho_i^m T_i^m B_i [(\sigma \cdot \sigma): \vec{n}_i \otimes \vec{n}_i - \sigma: \vec{n}_i \otimes \vec{n}_i \otimes \vec{n}_i \otimes \vec{n}_i \otimes \vec{n}_i \otimes \vec{n}_i)] \\ &+ 2 s_o \rho_i^w \sigma: \sigma_{ni}^w \vec{m}_i \otimes \vec{m}_i - s_o \rho_i^w (\sigma_{ni}^w)^2 \} \end{split}$$

The Gibbs energy accounts for the elastic deformation of the matrix and the displacement jumps of cracks, but not for the strain induced by crack growth (damage evolution). The inelastic strain $\boldsymbol{\varepsilon}^{\text{in}}$ is introduced in the expression of the total strain of the REV to account for the propagation of defects, as follows:

$$\varepsilon = \varepsilon^E + \varepsilon^{in} \tag{19}$$

(18)

where

$$\varepsilon^{E} = \frac{\partial G}{\partial \sigma} = \varepsilon^{e} + \varepsilon^{ed} \tag{20}$$

According to Eq. (18) and Eq. (20), ε^e and ε^{ed} can be calculated as:

$$\varepsilon^{e} = \frac{1 + v_{o}}{E_{o}} \sigma - \frac{v_{o}}{E_{o}} \operatorname{Tr}(\sigma) \delta \tag{21}$$

$$\varepsilon^{ed} = \sum_{i=1}^{Q} w_i \rho_i^m (s_1 T_i^m B_i^{\sim}_i : \sigma - \frac{1}{2} s_1 T_i^m \frac{\partial B_i}{\partial \sigma} \sigma : \sim_i : \sigma$$

$$+s_{o}N_{i}^{m} \quad _{i}:\sigma)+\sum_{i=1}^{Q}w_{i}\rho_{i}^{w}s_{o}\left(\frac{\partial\left(\sigma:\sigma_{ni}^{w}\vec{m}_{i}\otimes\vec{m}_{i}\right)}{\partial\sigma}-\sigma_{ni}^{w}\frac{\partial\sigma_{ni}^{w}}{\partial\sigma}\right)$$
(22)

where

$$_{ijkl} = n_i n_j n_k n_l \tag{23}$$

$$= \frac{1}{4} \left(n_i n_k \delta_{jl} + n_i n_l \delta_{jk} + n_j n_l \delta_{ik} + n_j n_k \delta_{il} \right) - n_i n_j n_k n_l$$
(24)

The damage driving force Y is calculated as the derivative of the Gibbs energy with respect to the crack density:

$$Y_i = \frac{\partial G}{\partial \rho_i} \tag{25}$$

3 DAMAGE CRITERION AND FLOW RULE

Both tensile stress and shear stress can lead to the growth of main cracks. We assume that the main cracks can propagate in either mode I or mode II, and the propagation criteria are given as:

$$f_{\rm li}^{\rm m} = \sigma_{ni}^{\rm m} \sqrt{\pi a_i^{\rm m}} - K_c \tag{26}$$

$$f_{\text{IIi}}^{\text{m}} = B_i \left\| \sigma_{ii}^{m} \right\| \sqrt{\pi a_i^{m}} - K_c \tag{27}$$

The tensile wing cracks can propagate in mode I, and the criterion is expressed as:

$$f_{li}^{\mathrm{w}} = \sigma_{ni}^{\mathrm{w}} \sqrt{\pi a_{i}^{\mathrm{w}}} - K_{c} \tag{28}$$

In order to account for the hardening of crack toughness, a hyperbolic function is used to express K_c (Jin & Arson, 2017):

$$K_c = \frac{a^{3/2}}{\frac{1}{K_o} + \frac{a}{\sigma_c}} \tag{29}$$

where $K_o = K_{Io}$ and $\sigma_c = \sigma_{Ic}$ for the mode I crack criterion; $K_o = K_{IIo}$ and $\sigma_c = \sigma_{IIc}$ for the mode II crack criterion; $a=a^{W}$ for wing cracks; $a=a^{M}$ for main cracks.

The crack radius is updated using the consistency rule:

$$da_i = -\frac{\partial f}{\partial \sigma} d\sigma / \frac{\partial f}{\partial a_i}$$
 (30)

By definition of the crack density (Eq.(6)), the crack density of crack family i can be updated as:

$$d\rho_i = \frac{2M_i a_i^2}{V_{\text{\tiny DEV}}} da_i \tag{31}$$

Due to the deformation, initiation and propagation of inter-granular cracks, geometric incompatibilities are noted around the cracks, which leads to crystals rearrangement. In order to account for the residual inelastic strains $\boldsymbol{\varepsilon}^{\text{in}}$, a discrete damage potential is introduced, as follows:

$$g_i = C_1 Y_i + C_o \tag{32}$$

The evolution law for the inelastic strain is obtained based on the damage potentials. Using a non-associative flow rule, we have:

$$\dot{\varepsilon}^{in} = \sum_{i=1}^{Q} \dot{\lambda}_{mi}^{in} \frac{\partial g_{mi}}{\partial \sigma} + \sum_{i=1}^{Q} \dot{\lambda}_{wi}^{in} \frac{\partial g_{wi}}{\partial \sigma}$$
 (33)

where λ_{mi}^{in} and λ_{vi}^{in} are the inelastic Lagrange multipliers for the main and wing cracks of family *i* respectively. The damage variable is also a function of the damage potential, as follows:

$$\dot{\rho}_{i} = \dot{\lambda}_{i}^{ed} \frac{\partial g_{i}}{\partial Y_{i}} = C_{1} \dot{\lambda}_{i}^{ed}$$
(34)

where λ_i^{ed} is damage Lagrange multiplier, assumed to be proportional to λ_i^{in} : $\lambda_i^{in} = C_i \lambda_i^{ed}$.

The global damage variable is defined as a second order tensor, and is calculated as the sum of the crack density tensors obtained for each family of cracks, as follows:

$$\Omega = \sum_{i=1}^{Q} \rho_{mi} \vec{n}_{i} \otimes \vec{n}_{i} + \sum_{i=1}^{Q} \rho_{wi} \vec{m}_{i} \otimes \vec{m}_{i}$$
(35)

4 CALIBRATION

The DFWCD model is calibrated against triaxial cyclic loading tests conducted on granular salt rock samples with 6% initial porosity, in dry conditions (Ding et al., 2017), as shown in Fig.3. Three loading cycles were applied to salt rock samples. The calibrated parameters are reported in Table 2.

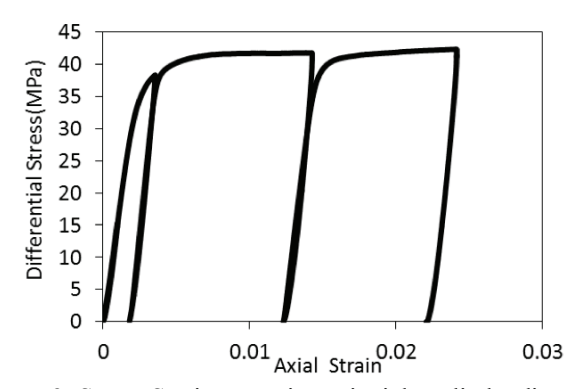


Figure 3. Stress-Strain curve in a triaxial cyclic loading test.

Table 2. Calibrated parameters for salt rock

Elasticity		Friction		Cracks geometry				
E_{o}	$E_{\rm c}$	ν_{o}	С	μ	$a_{ m mo}$	$M/V_{ m REV}$		
GPa	GPa	-	МРа	-	mm	mm^{-3}		
16	11	0.32	4	0.1	0.022	400		
Damage criterion								
K_{Ic}	K	Пс	$\sigma_{ m lc}$		$\sigma_{ m IIc}$	C_2		
MPa/n	nm M	Pa/mm	MP	Pa	MPa	-		
15	4(000	20		38	42		

Fig.4 shows the stress-strain curves obtained in the experiment and those obtained in the numerical simulations. During the first cycle, the stiffness is constant, until the deviatoric stress reaches 35MPa. Then, a sharp decrease of stiffness is observed. When the deviatoric stress exceeds 40MPa, salt rock exhibits a ductile behavior. Elastic stiffness decreases over the cycles, due to the accumulation of damage in the sample. In the proposed model, the inelastic strain is calculated from the damage potential. We note that the calibration of the model against stress/strain curves tends to slightly over predict the decrease of stiffness with damage and to

under-estimate the inelastic strain observed in the experiments. To overcome this limitation, it would be necessary to introduce a plastic potential, independent from the damage potential. Fig.5 presents the relation between lateral strain and deviatoric stress. As expected, the lateral strain induced by Poisson's effects is smaller than the axial strain.

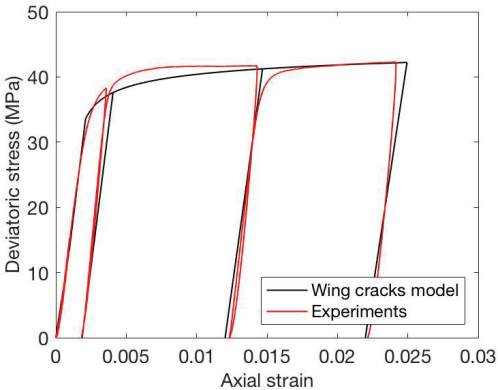


Figure 4. Calibration of the DFWCD model.

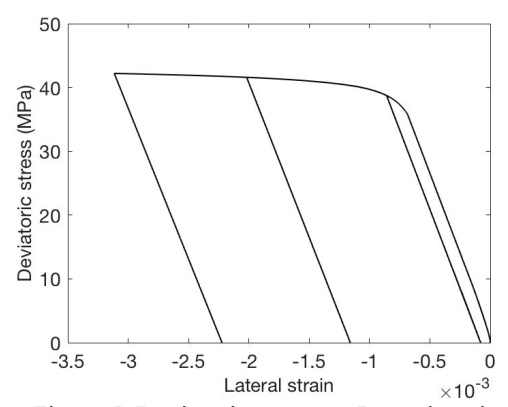
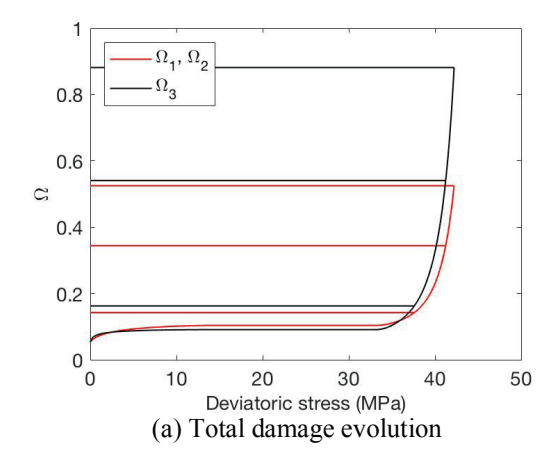
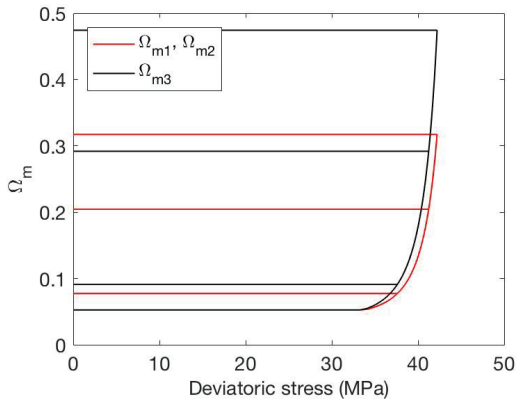


Figure 5. Deviatoric stress vs. Lateral strain.

The development of damage is shown in Fig.6. Damage accumulates when main cracks and wing cracks start to propagate. After damage initiation, the samples exhibit an anisotropic behavior. As shown in Fig.6(b), the damage of the main cracks is constant under low deviatoric stress. The largest damage of main cracks is observed in the direction of maximum compressive principal According to Fig.6(c), two stages of wing cracks damage evolution are observed. In stage one, the lateral damage due to wing cracks grows faster than the damage in the axial direction because the compressive axial stress is constraining the deformation of the sample. Vertical wing cracks develop due to shear stress in the matrix. In stage two, with the rapid growth of main cracks, the damage of wing cracks is controlled by the propagation of main cracks. Axial damage becomes larger than lateral damage. The damage stages of wing crack development are explained in Fig. 7.





(b) Damage evolution due to main cracks

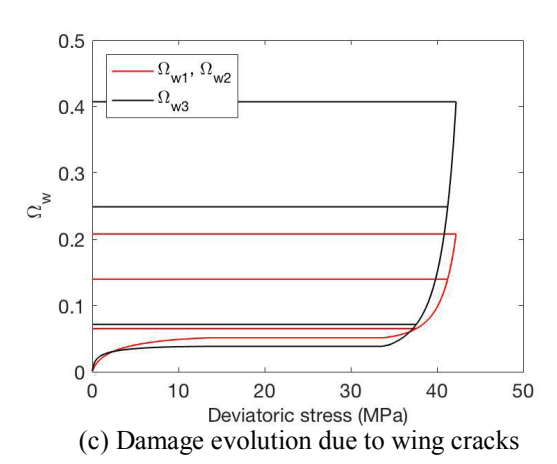


Figure 6. Damage evolution (Ω_3 is the damage in the direction of compressive principal stress; Ω_1 and Ω_2 are the lateral damage components).

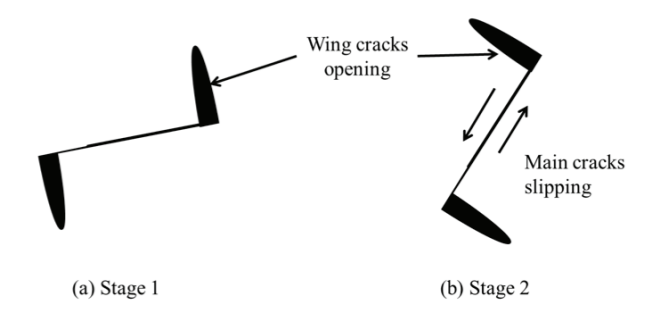


Figure 7. Damage stages of wing crack development.

5 CONCLUSION

A Discrete Frictional Wing Crack Damage (DFWCD) model is formulated to simulate the evolution of micro-cracks and the mechanical

behavior of salt rock. The stress-strain relationship at REV scale is related to the initiation and propagation of defects at micro scale.

REV defects include main cracks and wing cracks, which are assumed to be penny shaped. The Gibbs free energy is defined as the sum of the energy stored in the elastic matrix and in the cracks' displacement jumps. In order to simulate inter-crystalline bonding, a cohesive frictional model is used for the main cracks. The evolution of the main cracks is controlled by mode I and mode II fracture mechanics criteria. The growth of wing cracks is controlled by shear stresses in the matrix and in the main cracks, which generate tensile stress in the wing cracks. A mode I fracture criterion is used. The damage variable is defined as a crack density tensor; it is calculated by summing the crack densities obtained in 42 independent directions of space. An inelastic strain is introduced to account for the residual strain induced by the geometric incompatibilities around the cracks.

A triaxial cyclic loading test is used to calibrate the DFWCD model. The stiffness of the sample decreases with the accumulation of damage. The DFWCD model captures the degradation of stiffness over the cycles. When the deviatoric stress exceeds 40MPa, salt rock behaves as a ductile material. Mechanical anisotropy develops as damage accumulates.

The DFWCD model can be used to predict the initiation of micro-cracks, microstructure development, and damage evolution in crystalline materials. It can also be used to analyze the mechanical response of the host rock around geostorage facilities under complex loading paths. Future work will focus on extending the present model to include damage-plasticity couplings that are likely more important in recrystallized zero-porosity, polycrystalline rocks typical of natural salt bodies.

ACKNOWLEDGEMENTS

Financial support for this research was provided by the National Science Foundation (Grant No. CMMI-1362004/1361996).

6 REFFERENCES

- Arson, C., & Gatmiri, B., 2011. Thermohydromechanical modeling of damage in unsaturated porous media: Theoretical framework and numerical study of the edz, *International Journal for Numerical and Analytical Methods in Geomechanics*, vol. 36, no. 3, pp. 272–306.
- Bažant, P., Oh, B., 1986. Efficient numerical integration on the surface of a sphere. ZAMM-J. *Appl. Math. Mech./Zeitschrift für Angewandte Mathematik und Mechanik* 66 (1), 37–49.
- Budiansky, B., O'Connell, R.J., 1976. Elastic moduli of

- a cracked solid. Int. J. Solids Struct. 12 (2), 81-97.
- Cicekli, U., Voyiadjis, G. Z. and Al-Rub, R. K. A., 2007. A plasticity and anisotropic damage model for plain concrete, *International Journal of Plasticity*, vol. 23, no. 10, pp. 1874 –1900, In honor of Professor Dusan Krajcinovic.
- Ding, J., Chester, F. Chester, M. J., Shen, X. & Arson, C., 2017. Microcrack Network Development in Salt Rock During Cyclic Loading at Low Confining Pressure. 51st US Rock Mechanics/Geomechanics Symposium of the American Rock Mechanics Association, San Francisco, CA, June 25-28 2017, Paper 17-0308.
- Dyskin, A., Salganik, R., 1987. Model of dilatancy of brittle materials with cracks under compression. *Mech. Solids* 22 (6), 165–173.
- Germanovich, L., Salganik, R., Dyskin, A., Lee, K., 1994. Mechanisms of brittle fracture of rock with preexisting cracks in compression. *Pure Appl. Geophys*. 143 (1–3), 117–149.
- Jin, W. & Arson, C., 2017. Discrete equivalent wing crack based damage model for brittle solids, *International Journal of Solids and Structures*, Vol. 110–111, 279-293.
- Kachanov, M., 1992. Effective elastic properties of cracked solids: Critical review of some basic concepts, *Applied Mechanics Reviews*, vol. 45, no. 8, pp. 304–335.
- Kachanov, M.L., 1993. Elastic solids with many cracks and related problems. *Adv. Appl. Mech.* 30, 259–445.
- Kachanov, M.L., Shafiro, B., Tsukrov, I., 2013.Handbook of elasticity solutions. Springer Science & Business Media
- Lemaitre, J., & Desmorat, R., 2005. Engineering damage mechanics: Ductile, creep, fatigue and brittle failures. Springer Science & Business Media.
- Lehner, F., Kachanov, M., 1996. On modelling of "winged" cracks forming under compression. *Int. J. Fract.* 77 (4), R69–R75.
- Scholtès, L., Donzé, F.-V., 2012. Modelling progressive failure in fractured rock masses using a 3d discrete element method. *Int. J. Rock Mech.* Min. Sci. 52, 18–30.
- Zhu, C., & Arson, C., 2015. A model of damage and healing coupling halite thermomechanical behavior to microstructure evolution, *Geotechnical and Geological Engineering*, vol. 33, no. 2, pp. 389–410.